Inorganic Chemistry

Article

pubs.acs.org/IC

A Luminescent Poly(amidoamine)–Iridium Complex as a New Singlet-Oxygen Sensitizer for Photodynamic Therapy

Daniela Maggioni,[*,#,&,‡] Marco Galli,[#] Laura D'Alfonso,[§] Donato Inverso,[†,⊥] Maria Vittoria Dozzi,[#] Laura Sironi,[§] Matteo Iannacone,[†,⊥] Maddalena Collini,[§] Paolo Ferruti,[#,&] Elisabetta Ranucci,[#,&] and Giuseppe D'Alfonso[#,&]

[#]Dipartimento di Chimica, Università degli Studi di Milano, Via Golgi 19, 20133 Milano, Italy

[§]Dipartimento di Fisica, Università di Milano Bicocca, Piazza della Scienza 3, 20126 Milano, Italy

[†]Division of Immunology, Transplantation and Infectious Diseases, Dynamics of Immune Responses Unit, San Raffaele Scientific Institute, Via Olgettina 58, 20132 Milano, Italy

[⊥]Vita-Salute San Raffaele University, Via Olgettina 58, 20132 Milano, Italy

[&]Milan Research Unit, Consorzio Interuniversitario Nazionale per la Scienza e Tecnologia dei Materiali, Via Golgi 19, 20133 Milano, Italy

[‡]Institute of Molecular Science and Technologies, CNR, Via Golgi 19, 20133 Milano, Italy

Supporting Information

ABSTRACT: A polymer complex ($\mathbf{1_P}$) was synthesized by binding bis(cyclometalated) $Ir(ppy)_2^+$ fragments (ppy = 2-phenylpyridyl) to phenanthroline (phen) pendants of a poly(amidoamine) copolymer (PhenISA, in which the phen pendants involved ∼6% of the repeating units). The corresponding molecular complex $[Ir(ppy)_2(bap)]^+$ ($\mathbf{1_M}$, bap = 4-(butyl-4-amino)-1,10-phenanthroline) was also prepared for comparison. In water solution $\mathbf{1_P}$ gives nanoaggregates with a hydrodynamic diameter of 30 nm in which the lipophilic metal centers are presumed to be segregated within polymer tasks to reduce their interaction with water. Such confinement, combined with the dilution of triplet emitters along the polymer chains, led to $\mathbf{1_P}$ having a photoluminescence quantum yield greater than that of $\mathbf{1_M}$ (0.061 vs 0.034, respectively, in an aerated water solution) with a longer lifetime of the ^{3}MLCT excited states and a blue-shifted emission (595 nm vs 604 nm, respectively). NMR data supported segregation of the metal centers. Photoreaction of O_2 with 1,5-dihydroxynaphthalene showed that $\mathbf{1_P}$ is able to sensitize $^1O_2$ generation but with half the quantum yield of $\mathbf{1_M}$. Cellular uptake experiments showed that both $\mathbf{1_M}$ and $\mathbf{1_P}$ are efficient cell staining agents endowed with two-photon excitation (TPE) imaging capability. TPE microscopy at 840 nm indicated that both complexes penetrate the cellular membrane of HeLa cells, localizing in the perinuclear region. Cellular photodynamic therapy tests showed that both $\mathbf{1_M}$ and $\mathbf{1_P}$ are able to induce cell apoptosis upon exposure to Xe lamp irradiation. The fraction of apoptotic cells for $\mathbf{1_M}$ was higher than that for $\mathbf{1_P}$ (74 and 38%, respectively) 6 h after being irradiated for 5 min, but cells incubated with $\mathbf{1_P}$ showed much lower levels of necrosis as well as lower toxicity in the absence of irradiation. More generally, the results indicate that cell damage induced by $\mathbf{1_M}$ was avoided by binding the iridium sensitizers to the poly(amidoamine).

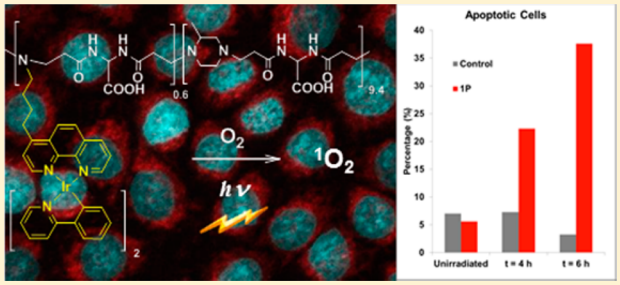

1. INTRODUCTION

Photodynamic therapy (PDT)[1] is receiving an increasing amount of attention as a noninvasive clinical treatment for different types of cancer[2] (such as those affecting skin,[3] bladder,[4] esophagus,[4] lung,[5] and head and neck[6]) and as an alternative method for killing pathogens in localized infections.[7]

PDT is based on the use of a photosensitizer (PS), which efficiently populates an excited triplet state upon interaction with visible light. The triplet state of a PS (^{3}PS*) can produce toxic reactive oxygen species (ROS), such as singlet oxygen ($^1O_2$) or free radicals, by two different pathways. ^{3}PS* can react with molecules to generate intermediate free radicals that in turn generate ROS (type I photochemistry). Alternatively, it can directly interact with molecular oxygen in its ground triplet state to produce "in situ" cytotoxic singlet oxygen ($^1O_2$) through an energy transfer process (eq 1).

$$^3PS^* + {}^3O_2 \rightarrow PS + {}^1O_2 \quad (1)$$

This type II photochemistry is the most relevant mechanism of PDT in cells, because most PSs are effective $^1O_2$ producers. The reactive oxygen species generated are capable of causing

Received: September 29, 2014

DOI: 10.1021/ic502378z
Inorg. Chem. XXXX, XXX, XXX−XXX

irreversible damage if generated inside cells, particularly inside specific subcellular organelles (mitochondria, Golgi apparatus, etc.) where the PSs can localize and accumulate. Indeed, singlet oxygen has a radius of destruction measured in nanometers (10−60 nm, its lifetime being in the range of 10−320 ns), and photodynamic damage will then occur only very close to the intracellular location of the PS.[8] Although dependent on many factors, only one of which is the subcellular location of the PS, PDT treatment can cause cell death by apoptotic or necrotic pathways, in dependence of many factors, including the subcellular location of the PS. Apoptosis is programed cell death that does not cause inflammation in vivo, whereas necrosis is a pathological cell death in which cellular content leaks out, potentially causing lethal damage in nearby cells and inflammation in vivo. In many cases, PDT has been found to be highly efficient at inducing apoptosis as a result of a complex cascade of events.[8,9] This feature is very important because it implies that doses lower than those necessary for producing necrosis may still be effective at killing cells.[10] Furthermore, efficient induction of apoptosis by PDT implies that PDT may be able to bypass mechanisms that make cells resistant to apoptosis in response to chemotherapeutic drugs and ionizing radiation.[10]

PDT would therefore be able to selectively kill diseased cells, reducing collateral effects on healthy tissues, provided that selective delivery of the PS to the target could be assured. Porphyrins,[1a,11] phthalocyanines,[1a] fullerene derivatives,[12] and organic dyes, like methylene blue[13] or rose bengal,[14] are valid PSs, as are some organometallic complexes.[1a] Among them, cyclometalated iridium complexes have attracted much attention[15−17] on the basis of many favorable properties: high quantum yields of triplet formation (even higher than 0.9 in deaerated solutions),[18] long lifetimes of the excited triplet state (typically in the microsecond range, which is long enough to enable quenching reactions with $^3O_2$ before spontaneous decay), and triplet energy high enough to allow for the energy transfer process (eq 1). Moreover, it has been shown that they are usually resistant to attack by singlet oxygen.[16]

However, several disadvantages hinder biomedical applications of these complexes. Their solubility in water is generally very low. Moreover, the circulating time of small molecules in biological fluids is generally too short to allow significant accumulation of a molecular sensitizer proximal to the target for in vivo applications.

The loading of complexes on suitable nanometric carriers can be exploited to improve their solubility in aqueous media, increase their plasma residence time, and reduce their toxicity.[1b,19] Actually, stealth nanoparticles (i.e., nanoparticles covered by macromolecules that make them invisible to the reticuloendothelial system) can benefit from a prolonged circulating time and effectively accumulate in solid tumors, owing to the so called enhanced permeability and retention (EPR) effect.[20]

Linear amphoteric poly(amidoamine)s (PAAs)[21] have well established properties of water solubility, biocompatibility, biodegradability, and stealth-like behavior.[22] Moreover, they tend to aggregate in water solutions in the form of small nanoparticles with hydrodynamic diameters in the range of 5−20 nm.[23,24] They are therefore very attractive as carriers for molecular complexes. In a previous work, a PAA copolymer (PhenISA, Chart 1) was synthesized bearing phenanthroline (phen) pendants,[24] which are strong chelating ligands toward a variety of transition-metal fragments. The phen ligand pendants

Chart 1. Structure of the PhenISA Copolymer

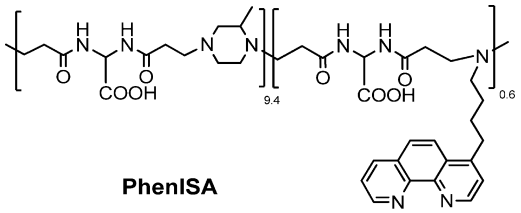

involved ∼6% repeating units, whereas the large majority of the units were those of the ISA23 polymer.[25] PhenISA was able to bind $Re(CO)_3^+$ and $Ru(phen)_2^{2+}$ fragments, affording luminescent polymer complexes that were internalized by HEK-293 cells.[24] These results prompted us to investigate the binding of PhenISA to iridium fragments to obtain a luminescent triplet emitter useful for both optical imaging and producing $^1O_2$ for PDT purposes.

This Article reports on the synthesis and photochemical characterization of a water-soluble Ir−PhenISA conjugate, showing that binding to the polymer improved the photophysical properties of the Ir emitters. The photooxidation of 1,5-dihydroxynaphthalene (DHN) was used to check the capability of this new metallopolymer to act as a sensitizer of $^1O_2$ generation. In preliminary tests with HeLa cells, the complex was internalized in cells and could be imaged by two-photon excitation microscopy. Moreover, the complex was able to induce cell apoptosis upon Xe lamp irradiation, with no evidence of the intrinsic cell damaging properties typically seen using the corresponding free Ir complex.

2. RESULTS AND DISCUSSION

2.1. Model Complex $[Ir(ppy)_2(bap)]^+$ ($\mathbf{1_M}$) (ppy = 2-phenylpyridyl, bap = 4-(butyl-4-amino)-1,10-phenanthroline). The related $[Ir(ppy)_2(phen)]^+$ complex was previously prepared by reacting dinuclear precursor $[Ir(ppy)_2Cl]_2$ with phen at high temperature in ethylene glycol.[26] In the polymer complex reported here, phen ligands are appended to the polymer chain by butylamino substituents in the 4-position of phenanthrolines (bap ligand, whose synthesis has been reported elsewhere).[24,27] It was therefore necessary to synthesize the $[Ir(ppy)_2(bap)]^+$ complex ($\mathbf{1_M}$) to have a reliable molecular model of the designed polymer complex. A previously published protocol was followed with some modifications (Scheme 1). The precursor $[Ir(ppy)_2Cl]_2$ was treated with 2 equiv of bap ligand in a mixed solvent (THF/H_2O 1:1) under mild heating (∼70 °C). A clear yellow solution formed upon heating, and the orange photoluminescence of the Ir complex progressively overcame the blue fluorescence of free phen. Reaction progress was monitored by ^1H NMR spectroscopy. All resonances were attributed by scalar and dipolar correlation two-dimensional $^1H-^1H$ and $^1H-^{13}C$ NMR experiments (Figures S1−S3 in the Supporting Information (SI)).

In contrast to the $[Ir(ppy)_2(phen)]^+$ complex, $\mathbf{1_M}$ (as a chloride salt) is moderately soluble in water due to the presence of a protonated amino group on the phen ligand (pK_a = 10.2, as determined by potentiometric titration on the bap ligand). Solubility was high enough to perform photophysical characterization in water solution, as well as the biological tests described in section 2.5. However, through dynamic light scattering (DLS) and NMR data, a minor fraction of the compound was

DOI: 10.1021/ic502378z
Inorg. Chem. XXXX, XXX, XXX−XXX

Scheme 1. Synthesis of Complex $\mathbf{1_M}$

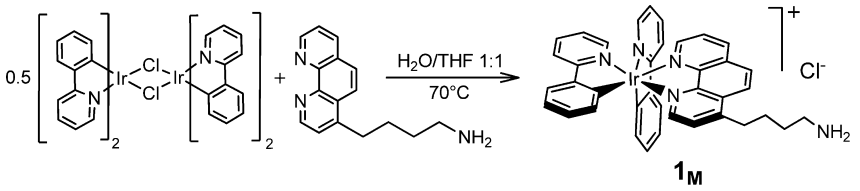

found to be present in the form of nanoaggregates, as discussed below.

The UV−vis absorption spectrum (Figure 1) of $\mathbf{1_M}$ shows strong spin-allowed ligand-centered (^{1}LC) bands in the range

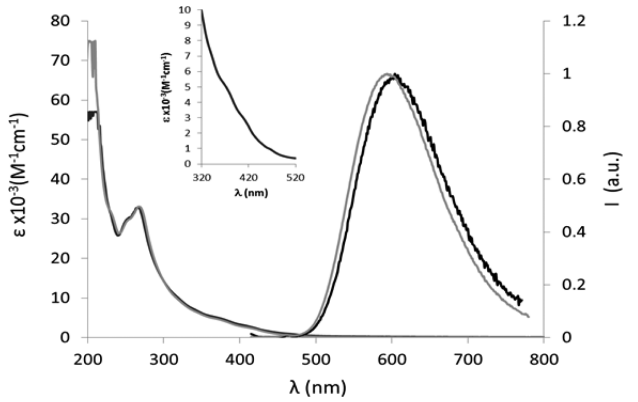

Figure 1. UV−vis absorption (left) and photoluminescence (right) spectra of $\mathbf{1_M}$ (black traces) and $\mathbf{1_P}$ (gray traces) in water at room temperature with λ_{ex} = 400 nm.

of 200−300 nm and broad weaker absorptions at longer wavelengths (peaks are recognizable at approximately 378 and 417 nm (Figure 1); their position did not change significantly upon varying the solvent, see Figure S4 in the SI), attributable to singlet metal-to-ligand charge transfer (^{1}MLCT) transitions, which is in agreement with literature data for similar complexes.[15,26,28]

Upon excitation at 400 nm, complex $\mathbf{1_M}$ exhibits yellow-orange photoluminescence at wavelengths that are strongly sensitive to the nature of the solvent (Table 1 and Figure S4 in the SI). A blue shift is observed upon decreasing solvent polarity,[29] which is typical of excited states that are more polar than their ground states (such as CT states) because they are preferentially stabilized by polar solvents, provided that the excited state lifetime is longer than the solvent reorganization time.[32,33] The sharp drop in the lifetimes (τ) and photoluminescence quantum yields (PLQYs, ϕ) in the presence of oxygen, observed in CH_2Cl_2 or CH_3CN solution (Table 1), indicates that emission occurs from an excited state with a substantially triplet nature. This agrees with literature data that attributed the emission from $[Ir(ppy)_2(phen)]^+$ complexes (phen indicating different phenanthroline-based ligands) as arising from ^{3}MLCT states involving the π^* orbitals of phen ligands as the acceptor orbitals.[26,28,34]

In water, $\mathbf{1_M}$ photoluminescence is centered at 604 nm, a position that did not change in the pH range of 3.2−7.2. The behavior in the presence of oxygen did not fit with the typical behavior of triplet emitters observed in organic solvents. Lifetimes and PLQYs were only modestly affected by the presence of oxygen (Table 1). Moreover, in aerated conditions, the PLQYs were higher in water than in acetonitrile, contrary to what would be expected from the polarity trend. A possible explanation was provided by DLS analysis of the water solution ($\sim 2 \times 10^{-5}$ M), which showed the presence of nanoparticles with hydrodynamic diameters of ∼200 nm. This suggested that $\mathbf{1_M}$ was not completely dissolved but was present, at least in part, in the form of nanosized aggregates. Such aggregates cannot account for the entirety of $\mathbf{1_M}$ present in solution because colloids are NMR silent (or give very broad, hardly detectable resonances),[35] whereas sharp ^{1}H NMR signals were observed for samples of $\mathbf{1_M}$ in water (e.g., Figure S1 of the SI). It has been shown (see Experimental Section) that the NMR silent fraction of $\mathbf{1_M}$ in water corresponds to ∼25% of the total sample. Such a fraction of aggregated $\mathbf{1_M}$, even if minor, could dominate the emission features because the complexes inside the nanoparticles are expected to be more brilliant, being protected from the deactivating actions of oxygen and the polar solvent.[36] Therefore, the wavelength, lifetime, and PLQYs of the emission measured in water should be primarily attributed to the aggregates, with little contribution from the free molecules. Interestingly, in water, a double exponential model was necessary to describe the lifetime decays (Table 1) to achieve a function of merit (χ^2) comparable to that obtained for the organic solvents. The main component (longer and less sensitive to oxygen) is ascribable to the species inside the

Table 1. Photoluminescence Data for Molecular Complex $\mathbf{1_M}$ in Aerated or Deaerated Solutions in Different Solvents and for Polymer Complex $\mathbf{1_P}$ in an Aerated Water Solution[a]

compound	solvent	λ_{em} (nm)	condition	τ (ns)	ϕ	k_r (s^{-1})	k_{nr} (s^{-1})
$\mathbf{1_M}$	CH_2Cl_2	574	aerated	153	0.052	3.4×10^5	6.2×10^6
			deaerated	1123	0.35	3.1×10^5	5.8×10^5
$\mathbf{1_M}$	CH_3CN	591	aerated	56	0.017	3.1×10^5	1.8×10^7
			deaerated	858	0.30	3.5×10^5	8.2×10^5
$\mathbf{1_M}$	H_2O	604	aerated	116 (98%), 2 (2%)	0.033	2.8×10^{5b}	8.3×10^{6b}
			deaerated	134 (95%), 64 (5%)	0.038	2.8×10^{5b}	7.2×10^{6b}
$\mathbf{1_P}$	H_2O	595	aerated	212	0.061	2.9×10^5	4.5×10^6

[a]Room temperature, λ_{ex} = 400 nm; k_r and k_{nr} indicate the radiative and nonradiative decay constants of the excited states, respectively. [b]Computed on the most significant lifetime component.

DOI: 10.1021/ic502378z
Inorg. Chem. XXXX, XXX, XXX−XXX

Scheme 2. Synthesis of the Polymer Complex $\mathbf{1_P}$

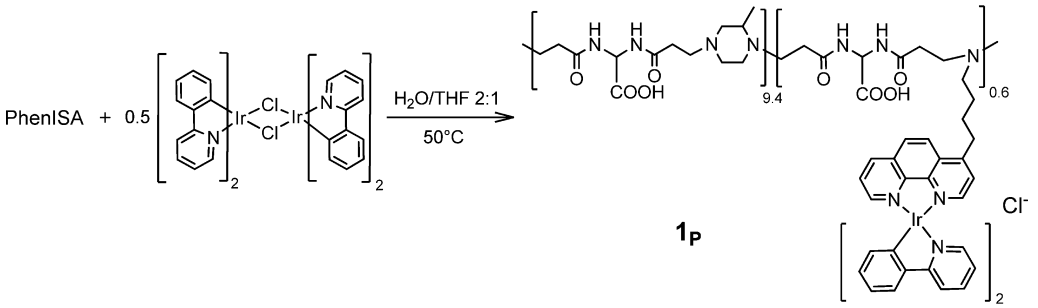

nanoparticles, whereas the minor component (shorter and strongly affected by oxygen) is attributable to free molecules.

2.2. Preparation and Characterization of the $\mathbf{1_P}$ Complex. Synthesis of the PhenISA copolymer (Chart 1) has been previously reported.[24] The majority of it is derived from a Michael addition reaction between piperazine and bis(acrylamido)acetic acid (BAC), whereas a minority piece (~6%) arises from the analogous reaction between BAC and the primary amine bap. DLS measurements indicated that this copolymer self-assembled in aqueous media, giving rise to the formation of roughly spherical nanoaggregates with a hydrodynamic diameter of ~20 nm.[24]

Complexation of Ir to PhenISA was performed by a route similar to that used for preparing molecular complex $\mathbf{1_M}$ (Scheme 2), but in a THF/H_2O mixed solvent containing double the amount of water with respect to the synthesis of $\mathbf{1_M}$ because of the low solubility of PhenISA in nonaqueous media. On the other hand, the presence of THF was necessary because starting reagent $[Ir(ppy)_2Cl]_2$ is insoluble in water. The reaction temperature was lower (50 °C) than that used for the synthesis of $\mathbf{1_M}$ to avoid thermal degradation of the polymer. After 6.5 h, the mixture was concentrated under reduced pressure to remove most of the THF and dialyzed against water for four days to remove unreacted metal fragments and lower molecular weight polymer fractions, if present.

The content of Ir bound to the polymer was measured by ICP-AES analysis. The results (2.45% w/w) indicated that the majority (88.3%) of the phenanthroline pendants had reacted with $Ir(ppy)_2$ fragments.

Binding of the metal centers did not hamper the tendency of PhenISA to self-aggregate. A DLS measurement, performed on a sample of dialyzed and lyophilized $\mathbf{1_P}$, showed a size distribution centered at ~30 nm (Figure S5 in the SI), which is slightly larger than that of PhenISA alone.

Another interesting feature of the organization of the polymer coils in solution was revealed by the ^{1}H NMR spectrum of the purified polymer complex $\mathbf{1_P}$ in D_2O solution. In these conditions, the aromatic resonances of the ppy and phen ligands were particularly broad, and their integrated intensities did not reflect the true percentage of the minority component (see the bottom spectrum of Figure S6 in the SI, in which the aromatic signals are almost undetectable). Progressive addition of THF-d_8 to the NMR tube led to the recovery of the aromatic resonances at their correct intensities (Figure S6 in the SI). This suggests that, in water, the complexes, in which the metal is surrounded by a lipophilic cage formed by the three large aromatic ligands, tend to segregate within the polymer to avoid contact with the water. Upon the less polar THF solvent being added, segregation was relieved, and exposure to the mixed solvent made the $Ir(ppy)_2(bap)$ pendants more mobile and consequently their ^{1}H signals more visible.

The UV−vis absorption spectrum of $\mathbf{1_P}$ was superimposable on that of molecular complex $\mathbf{1_M}$, except for the very intense absorption at ~200 nm due to the amide groups of the polymer (gray trace in Figure 1). The photoluminescence spectrum instead showed some significant differences with respect to that of $\mathbf{1_M}$. The emission maximum was blue-shifted by 9 nm (250 cm^{-1}), and a longer lifetime (212 ns) and higher quantum yield (0.061) were found. These findings agree with the idea that, in water, the pendant Ir complexes are segregated into polymer pockets in which they experience less polar surroundings (thus giving a blue-shifted emission) and a more rigid environment than in solution. Moreover, the emitting Ir centers are very diluted along the polymer chains of $\mathbf{1_P}$ because the units bearing the phen pendants are a very minor component of the copolymer. This prevents self-quenching and annihilation effects, which are often encountered for emission from the triplet state of transition-metal complexes in solids or in films at high dopant concentrations[37] and might also occur in the nanoaggregates formed by $\mathbf{1_M}$ in water. In fact, the best emitting features are often observed in systems where a rigid environment (rigidochromic effect)[38] is joined to a low dopant concentration.[39]

2.3. Photochemical Stability of $\mathbf{1_P}$. Photochemical stability tests were carried out to determine the robustness of both the iridium complex and the PAA chain under prolonged irradiation in the presence of O_2. This is a key prerequisite for using the polymer complex as a photosensitizer. $\mathbf{1_P}$ was dissolved in water/methanol (85:15), and the solution was saturated with oxygen by bubbling O_2 for 10 min. The solution was then exposed to visible light (150 W xenon lamp, 390 nm cutoff filter), and UV−vis absorption spectra were recorded every 30 min for 4 h (Figure S7 of the SI). Superposition of the absorption spectra recorded at different times revealed high photostability of the compound. The same test was repeated for complex $\mathbf{1_M}$ with analogous results.

2.4. Photoreaction of $\mathbf{1_P}$ and $\mathbf{1_M}$ with 1,5-Dihydroxynaphthalene as a Reporter of $^1O_2$ Formation. To test the capability of $\mathbf{1_M}$ and $\mathbf{1_P}$ to act as sensitizers for $^1O_2$ generation, photochemical reactions were performed in solutions presaturated with O_2, employing 1,5-dihydroxynaphthalene (DHN) as the $^1O_2$ reporter. Indeed, it is known that DHN promptly and quantitatively reacts with $^1O_2$ to give 5-hydroxy-1,4-naphthalenedione (juglone, Scheme 3).[15,40]

Reaction progress was monitored by UV−vis absorption spectroscopy following the decrease in the DHN band at 297 nm and the concomitant increase of the large juglone band centered at 427 nm (Figure 2). This reaction occurred without

DOI: 10.1021/ic502378z
Inorg. Chem. XXXX, XXX, XXX−XXX

Scheme 3. Photochemical Reaction Used To Monitor $^1O_2$ Formation[a]

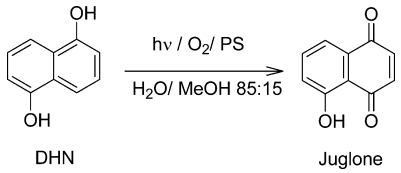

[a]PS represents the Ir complexes $\mathbf{1_M}$ and $\mathbf{1_P}$.

the formation of long-lived intermediates or byproducts as indicated by the two isosbestic points at 280 and 330 nm observed in the spectra recorded during the course of the irradiation. Negligible juglone formation was observed in the absence of the Ir sensitizers, even after 70 min of irradiation of O_2-saturated solutions.

Figure 3 shows the first-order semilogarithmic plots for reaction 2, sensitized by either $\mathbf{1_M}$ or $\mathbf{1_P}$. In the case of $\mathbf{1_M}$, the values of $\ln(A_t/A_0)$ decreased linearly over time from the beginning up to ~50 min of irradiation, in agreement with pseudo-first-order kinetics, with rate $r = k_{obs}[DHN]$ (slope = $k_{obs} = 5.1 \times 10^{-3}$ min^{-1}). At longer times, progressive deviation from linearity was observed, possibly related to the fact that juglone absorbs at the same wavelengths as the Ir sensitizer. The rate of juglone formation compares well with that observed for the same reaction sensitized by the $[Ir(ppy)_2(phen)]^+$ complex in a mixed acetonitrile/2-PrOH solution ($k_{obs} = 6 \times 10^{-3}$ min^{-1}).[40]

$$DHN + {}^1O_2 \rightarrow \text{juglone} + \frac{1}{2}{}^3O_2 \qquad (2)$$

On the contrary, an induction period was observed for $\mathbf{1_P}$, followed by a linear decrease with a smaller slope ($k_{obs} = 2.1 \times 10^{-3}$ min^{-1}). The induction time suggests that at the beginning the polymer itself competed with DHN for consuming $^1O_2$, most likely by reaction with the alkene groups[41] constituting the terminals of the PAA chains (obtained by Michael addition reactions). Therefore, reaction 2 likely could only start when these terminal groups had been saturated. The lower rate relative to $\mathbf{1_M}$ is probably attributable to the fact that quenching

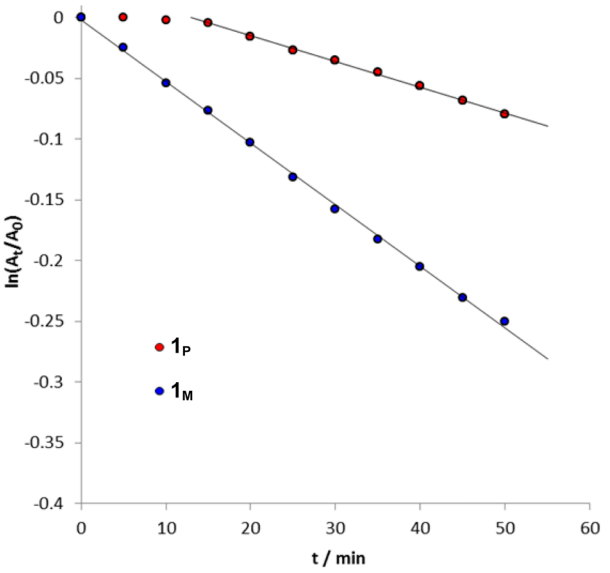

Figure 3. Photooxidation of DHN in the presence of sensitizers $\mathbf{1_M}$ and $\mathbf{1_P}$ (data up to 50 min have been plotted corresponding to the linearity time interval). A_t and A_0 represent the absorbance measured at 297 nm (the maximum of the DHN absorption band) at time t and time 0, respectively. The absorbance of the Ir sensitizer at this wavelength was subtracted.

of excited triplet sensitizers by $^3O_2$ (reaction 1) requires the interaction of the two species, and the mobility of the Ir complexes in $\mathbf{1_P}$ is drastically reduced with respect to that of $\mathbf{1_M}$ because of their binding to the polymer. Furthermore, the photophysical and NMR data suggest that the polymer adopts conformations that favor segregation of the complexes to reduce its interaction with water. Therefore, the time necessary for the generated $^1O_2$ to diffuse in the solution and encounter the DHN probe must also be considered.

The ratio between the slopes of the two lines reported in Figure 3, corrected to take into account the different amount of radiation absorbed by the two sensitizers during the reaction, allowed for the ratio of the quantum yields of $^1O_2$ generation by $\mathbf{1_M}$ and $\mathbf{1_P}$ to be estimated as 2.1 (see Experimental Section for details). Thus, binding to the polymer reduces the efficiency of

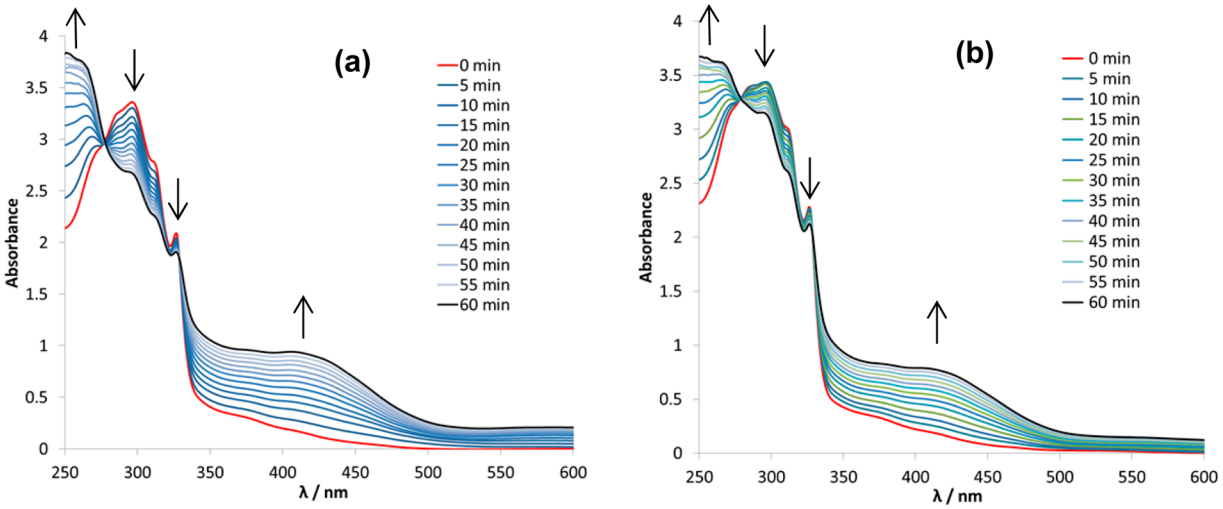

Figure 2. UV−vis absorption spectra recorded at different times of irradiation ($\lambda > 390$ nm, xenon lamp) on solutions containing (a) complex $\mathbf{1_M}$ (4.1×10^{-5} M) or (b) complex $\mathbf{1_P}$ (3.6×10^{-5} mol/L of Ir) and DHN (3.7×10^{-4} M) in 3 mL of H_2O/MeOH (85:15) bubbled with O_2 for 10 min.

DOI: 10.1021/ic502378z
Inorg. Chem. XXXX, XXX, XXX−XXX

the Ir complex as a sensitizer for $^1O_2$ generation, though not dramatically.

2.5. PDT Treatment of Cells. Before testing the capability of the Ir complexes to induce cell death by $^1O_2$ generation, we investigated their cellular uptake. The efficiency of photosensitizer incorporation into the cells can significantly affect the capability of the sensitizer to induce cell death.[14] Therefore, HeLa cells were incubated with compounds $\mathbf{1_M}$ and $\mathbf{1_P}$ at 37 °C under a 5% CO_2 atmosphere (see Experimental Section) for differing amounts of time. Images of the incubated cells were then acquired by two-photon excitation (TPE) microscopy at 840 nm, where both complexes showed the highest two-photon absorption. TPE allows for less cellular damage and deeper light penetration in vivo because typical laser wavelengths lie in the 700−900 nm range corresponding to the window in which both the tissue chromophores and water absorb more weakly.

Previous studies had shown that cellular internalization of the Ru−PhenISA complex required several hours.[24] Uptake of Ir−PhenISA complex $\mathbf{1_P}$ was therefore checked after 12 h of incubation. However, uptake of molecular complexes is usually faster;[42] therefore, internalization of $\mathbf{1_M}$ was monitored after 2 h of incubation.

Figure 4 shows that both molecular complex $\mathbf{1_M}$ (upper panels) and polymer complex $\mathbf{1_P}$ (lower panels) are able to

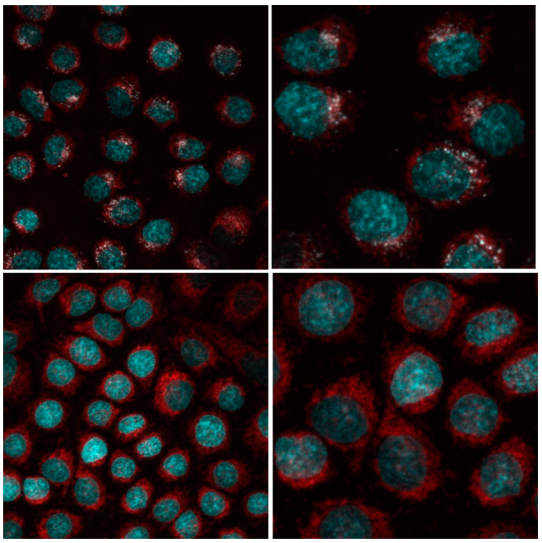

Figure 4. TPE microscopy images (superposition of the blue and red channels) of HeLa cells incubated for 2 h with 26 μM $\mathbf{1_M}$ (upper panels) or for 12 h with 22 μM $\mathbf{1_P}$ (lower panels) and counterstained with Hoechst to visualize the nuclei in the blue channel. The red color is due to the Ir complexes. An image of control HeLa cells (incubation without Ir complexes) for this experiment is shown in Figure S8 in the SI. Left panels: 157 × 157 μm^2; right panels: enhanced to 79 × 79 μm^2.

penetrate the cellular membrane and that both tend to be located in the perinuclear region. This is in line with literature data concerning related bis(cyclometalated) Ir complexes, in which localization in subcellular organelles, such as the Golgi apparatus, endoplasmic reticulum, lysosomes, and mitochondria, was suggested.[17b,d,e,43]

These preliminary experiments therefore indicated that $\mathbf{1_P}$ is an efficient cell staining agent endowed with TPE imaging capability that is well tolerated by cells. Indeed, cells still appeared viable after the long incubation time, which was further confirmed by quantification of dead cells on nonirradiated samples as described below.

For PDT tests, HeLa cells were incubated with $\mathbf{1_M}$ or $\mathbf{1_P}$ as described above for the cellular uptake assays. Subsequently, multiwell plates were irradiated for 5 min with a Xe lamp and then maintained at 37 °C under a 5% CO_2 atmosphere (see Experimental Section). The same treatment was applied to control cells (without sensitizer) to check for adverse effects of exposure to the Xe lamp. Cell viability was evaluated by flow cytometry analysis performed 4 and 6 h after irradiation along with nonirradiated samples (Figure S9 of SI) using annexin V and 7-aminoactinomycin D (7AAD) staining to denote apoptotic and necrotic cells, respectively.

Cells incubated with either $\mathbf{1_M}$ or $\mathbf{1_P}$ underwent apoptosis upon irradiation (Figure 5). The fraction of apoptotic cells for

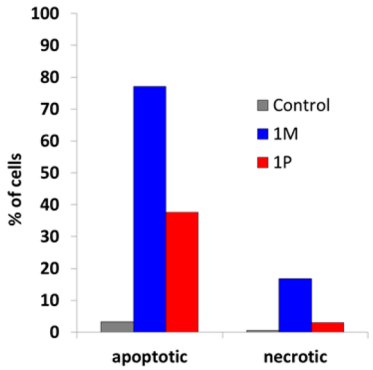

Figure 5. Percentages of dead cells resulting from apoptotic or necrotic events upon PDT treatments (6 h after being irradiated for 5 min) in control samples and samples sensitized by $\mathbf{1_M}$ or $\mathbf{1_P}$.

$\mathbf{1_M}$ was higher than that for $\mathbf{1_P}$, which is in line with the kinetics of $^1O_2$ generation measured in the photooxidation of DHN. However, an increased number of necrotic events with respect to the untreated cells were observed in the cells treated with $\mathbf{1_M}$ (Figure 5 and Figure S9 of the SI).

Next, to investigate dark toxicity (i.e., toxicity in the absence of irradiation), HeLa cells were incubated with either $\mathbf{1_M}$ or $\mathbf{1_P}$, and the number of viable (living cells recovered after treatment) and dead cells was measured (see Experimental Section). As shown in Figure S10 of the SI, cells treated with $\mathbf{1_M}$ had a significantly higher number of dead cells and a significant reduction in cell viability relative to both untreated and $\mathbf{1_P}$-treated cells.

Therefore, taken together, these results indicate that treatment with free complex $\mathbf{1_M}$ has a significant cytotoxic effect even without exposure to the Xe lamp. Cells incubated with $\mathbf{1_P}$ showed much less cytotoxicity (both in the dark and upon irradiation). Interestingly, binding of the sensitizer to poly(amidoamine) inhibited necrosis upon irradiation while preserving its ability to induce apoptosis.

3. CONCLUSIONS

The new luminescent metallopolymer $\mathbf{1_P}$ presented here is of interest in several respects. Upon light absorption, bis(cyclometalated) Ir complexes appended to the polymer give rise to triplet metal-to-ligand charge transfer excited states that can either radiately decay or react with $^3O_2$ and can then be exploited for either imaging or PDT applications. It has been found that photoluminescence can be triggered by two-photon excitation, which offers advantages over traditional one-photon

DOI: 10.1021/ic502378z
Inorg. Chem. XXXX, XXX, XXX−XXX

excitation in terms of less cellular damage and deeper light penetration in vivo. Moreover, preliminary tests have shown that $\mathbf{1_P}$ is internalized by living HeLa cells, which is an important asset for PDT applications. Therefore, from the point of view of imaging applications, $\mathbf{1_P}$ provides an efficient water-soluble cell staining agent capable of TPE imaging that is well tolerated by cells.

Moreover, binding to the polymer improved the photophysical properties of the Ir complexes, doubling their lifetimes and photoluminescence quantum yields, most likely because the metal centers, being buried within lipophilic ligand cages, are diluted and segregated into polymer tasks in an environment that is more rigid and somewhat protected from water (and possibly from O_2). In fact, several examples reported in the literature have used similar approaches to shield triplet excited states from quenchers that would prevent applications in bioimaging or photocatalysis.[44]

Notably, in the present case, segregation did not hinder the ability of the Ir complexes contained in $\mathbf{1_P}$ to sensitize $^1O_2$ generation. The rate of $^1O_2$ generation for $\mathbf{1_P}$ was lower than that for the free complex $\mathbf{1_M}$ as shown by photooxidation of DHN, but the rate difference was not dramatic. Then, $\mathbf{1_P}$ maintained the capability of inducing apoptosis by irradiation for a short time in a large fraction of irradiated cells. The percentage of dead cells was lower than that observed in the PDT tests sensitized by $\mathbf{1_M}$, but $\mathbf{1_P}$ caused much less necrosis than $\mathbf{1_M}$. Thus, the experiments reported here indicate that binding of the Ir sensitizers to the PhenISA copolymer allows them to avoid the significant cellular damage caused by the free complex $\mathbf{1_M}$.

This is just one of the beneficial effects expected from the binding of metal emitters to poly(amidoamine)s, whose biocompatibility has already been evidenced.[22] Moreover, for in vivo applications, it is expected that binding of the sensitizers to a nanometric carrier will increase their circulating time and favor their effective accumulation into solid tumors by the EPR effect.

The present work therefore provides proof of principle that binding of Ir triplet emitters to poly(amidoamine)s affords conjugates with potential as both cell imaging agents and sensitizers of $^1O_2$ generation. For improving such potential as it relates to clinical applications, further work will be necessary to tailor the ligand sphere of the metal and to shed light on the mechanism of cellular penetration and intracellular localization.

4. EXPERIMENTAL SECTION

4.1. Materials. 2-Methylpiperazine was purchased from Fluka and purified by sublimation, with final purity (98%) determined by acidimetric titration. *N*,*N*′-Bis(acrylamido)acetic acid (BAC) was prepared following a method previously published in the literature,[45] and purity (98%) was determined by NMR spectroscopy and titration. $[Ir(ppy)_2Cl]_2$ was prepared using a published method[46] with $IrCl_3 \cdot 3H_2O$ as a precursor (BASF). All the other reagents were obtained from Aldrich and used as received, if not otherwise specified. THF was distilled from Na/benzophenone using standard Schlenk techniques. Ultrapure water (Milli-Q, Millipore, resistivity = 18 M Ω cm^{-2}) was used for the preparation of the aqueous solutions. D_2O (99.9%) was purchased from Aldrich and used as received; THF-d_8 (99.9%) was purchased from CIL.

4.2. Instruments and Methods. NMR experiments were performed on a Bruker DRX400 spectrometer equipped with a Bruker 5 mm BBI *Z*-gradient probe head with a maximum gradient strength of 53.5 G/cm.

DLS measurements were performed using a Malvern Zetasizer nano ZS instrument at 289 K on samples dissolved in ultrapure water (typically 1 mg/mL).

Elemental C, H, N analyses were performed on a PerkinElmer CHN 2400 instrument. Ir content was determined by ICP-AES (ICAP 6300, Thermo Electron) on a known amount of $\mathbf{1_P}$ dissolved in 1.5 mL of 30% HCl (Suprapur) and 0.5 mL of 65% HNO_3 (Suprapur), digested overnight at room temperature, and finally diluted to 10 mL with ultrapure water in a volumetric flask.

UV−vis absorption spectra were acquired on an Agilent model 8543 spectrophotometer at room temperature. Determination of the molar absorptivity (ε) values of the ^{1}MLCT transitions for $\mathbf{1_P}$ was performed by dissolving an accurately weighted amount of $\mathbf{1_P}$ (balance with readability up to 0.01 mg) in a volumetric flask and calculating the Ir content on the basis of ICP-AES analyses.

Steady state photoluminescence measurements were performed on a Horiba−Jobin−Yvon Fluorolog spectrometer, correcting the emission spectra for the spectroscopic sensitivity of the photomultiplier tube. Quantum yields were determined using $[Ru(bpy)_3]Cl_2$ as a standard (ϕ = 0.04 in aerated water solutions).[47] Values of the radiative constants k_r have been obtained from the ϕ/τ ratio, assuming the efficiency of the intersystem crossing process is equal to 1.

Lifetimes were measured by frequency-domain methods. A frequency modulated phase fluorometer (Digital K2, ISS) was employed using a laser diode at 378 nm as an excitation source. At least 15 data points were acquired at logarithmically spaced frequencies in the range of 0.3−60 MHz with a cross correlation frequency of 400 Hz. The convenient accuracies for phase angles and modulation ratios were 0.2° and 0.004, respectively. Lifetime measurements were performed under the magic angle conditions, and a 535 nm long pass filter (Andover Co.) was employed to cut light scattering. A solution of glycogen in doubly distilled water was used as the reference sample. Lifetime data fitting was accomplished by an ISS routine based on Marquardt least-squares minimization. In the case of multiple exponential components in the decay scheme, the fit of the fluorescence intensity decay $F(t)$ yields lifetime values (τ_i) together with corresponding fractional intensities (f_i): $F(t) = \sum \alpha_i e^{-t/\tau_i}$ and $f_i = \alpha_i\tau_i/\sum \alpha_i\tau_i$, where α_i represent pre-exponential factors. The value of the fractional intensities for each component is proportional to the molar extinction coefficient (ε_i), the concentration (c_i), and the quantum yield (ϕ_i) of the component, $f_i \propto \varepsilon_i c_i \phi_i$.

The typical error affecting lifetime measurements is about 5%, with the exception of longer lifetimes (i.e., >500 ns), for which the error rises to ∼10% due to the nonoptimal working frequency range available for the amplifiers. In organic solvents, lifetime decay data were satisfactorily described by a simple single exponential model; fitting of the data yielded χ^2 values on the order of 5 with no trends in the residue plot (deviation of the χ^2 from unity is mainly due to the poor performance of the amplifiers at 0.3 MHz; their working range spans the interval 0.1−300 MHz). As stated above, a double exponential model had to be assumed to describe the lifetime decay in water to achieve a function of merit (χ^2) comparable to that obtained for the organic solvents.

The photochemical stability test and photoreaction with DHN in the presence of $\mathbf{1_M}$ and $\mathbf{1_P}$ employed a Jasco V-650 spectrophotometer. The experiments were performed in a 3 mL quartz cuvette inserted into a homemade housing that consists of a black box mounted on an optical bench. The irradiation source was an Osram Powerstar HCI-T with a 150 W/NDL lamp mounted on a Twin Beam T 150 R reflector that primarily emits visible light above 400 nm, with a small emission in the 350−400 nm range that was eliminated after placing a 390 nm cutoff filter at the black box entrance (Figure S10 in the SI). The lamp and reactor were separated by a fixed distance of 10 cm. The whole setup was maintained at ambient temperature by a continuous stream of air.

4.3. Synthesis of Model Complex [Ir(ppy)$_2$(bap)]Cl ($\mathbf{1_M}$·Cl). In a Schlenk tube, 34.7 mg of $[Ir(ppy)_2Cl]_2$ (3.24×10^{-2} mmol) was dissolved in 9 mL of anhydrous, freshly distilled THF. A solution of 4-(butyl-4-amino)-1,10-phenanthroline[24,27] (bap, 16.2 mg, 6.45×10^{-2} mmol) in water (9 mL) was then added at room temperature. The

DOI: 10.1021/ic502378z
Inorg. Chem. XXXX, XXX, XXX−XXX

mixture was heated at 70 °C. The starting turbid suspension rapidly turned to a clear yellow solution, and the color observed under UV irradiation changed from blue (fluorescence of free phen) to orange following the formation of the luminescent Ir complex. Reaction progress was monitored by ^{1}H NMR spectroscopy. Heating was stopped after 5 h, and the mixture was stirred overnight. The solvent was evaporated under vacuum, and the product was isolated by precipitation from THF/Et_2O (1:2) and dried under vacuum. Final treatment of the solid with Et_2O (2 mL × 3) followed by vacuum evaporation to dryness gave $\mathbf{1_M}$·Cl. Isolated yield: 69%. UV−vis (H_2O) MLCT absorptions: λ_{abs} 378 nm (ε = 4690 M^{-1} cm^{-1}) and 417 nm (ε = 2610 M^{-1} cm^{-1}). ^{1}H NMR (D_2O, 300 K, 9.4 T): δ 8.60 (1H, C*H*(9), dd, J = 8.5, 1.0 Hz), 8.33 (1H, C*H*(5), d, J = 9.5 Hz), 8.30 (1H, C*H*(7), dd, J = 5.2, 1.0 Hz), 8.18 (1H, C*H*(2), d, J = 5.3 Hz), 8.16 (1H, C*H*(6), d, J = 9.5 Hz), 8.02 (2H, C*H*(6′), pseudo d, J = 7.9 Hz), 7.85 (2H, C*H*(3″), d, J = 7.6 Hz), 7.75 (2H, C*H*(5′), m), 7.70 (1H, C*H*(8), dd, J = 8.5, 5.2 Hz), 7.58 (1H, C*H*(3), d, J = 5.3 Hz), 7.40 (2H, C*H*(3′), pseudo t, J_{app} = 6.7 Hz), 7.08 (2H, C*H*(4″), pseudo t, J_{app} = 7.2 Hz), 6.95 (2H, C*H*(5″), pseudo t, J_{app} = 7.2 Hz), 6.80 (2H, C*H*(4′), pseudo t, J_{app} = 6.7 Hz), 6.46 (2H, C*H*(6″), d, J = 7.4 Hz), 3.28 (2H, C*H*(δ), t, J = 7.00 Hz), 2.95 (2H, C*H*$_2$(α), t, J = 7.30 Hz), 1.82 (2H, C*H*$_2$(γ), m), 1.72 (2H, C*H*$_2$(β), m). ^{13}C NMR (D_2O, 300 K, 9.4 T): δ 151.4 (CH(5)), 150.5 (CH(2)), 149.0 (CH(3′)), 138.4 (CH(9)), 138.4 (CH(5′)), 131.9 (CH(6″)), 130.5 (CH(5″)), 127.9 (CH(6)), 126.2 (CH(8)), 125.9 (CH(8)), 124.9 (CH(3″)), 124.1 (CH(7)), 127.9 (CH(6)), 123.3 (CH(4′)), 122.6 (CH(4″)), 119.8 (CH(6′)). FAB-MS m/z: calcd for $C_{38}H_{33}N_5Ir$ [M+], 752; found, 752 (with the expected isotopic pattern). Elemental analysis: Anal. Calcd for $C_{38}H_{33}N_5IrCl$: C, 57.97; H, 4.22; N, 8.89. Found: C, 57.52; H, 4.35; N, 8.73. For determining the amount of NMR silent $\mathbf{1_M}$ (i.e., $\mathbf{1_M}$ present in the form of nanoaggregates), a sample of $\mathbf{1_M}$ (∼1 mg) was dissolved in CD_2Cl_2 in an NMR tube, and the intensities of its resonances were calibrated against an internal standard (CH_3CN, 1 μL). The solution was evaporated to dryness in the NMR tube. The residue was dissolved in D_2O; 1 μL of standard was added, and the calibration was repeated, showing intensities of the resonances corresponding to ∼75% with respect to those of the CD_2Cl_2 solution.

4.4. Preparation and Characterization of $\mathbf{1_P}$. A water solution (2 mL) of PhenISA (57.3 mg, 7.29 × 10^{-3} mmol of bap) was treated with 1 mL of a THF solution containing 4.6 mg of $[Ir(ppy)_2Cl]_2$ (4.29 × 10^{-3} mmol, 1.15 equiv), giving a turbid solution that became clear as the temperature rose to 50 °C. The yellow color of the solution did not change significantly during the reaction, whereas under UV illumination, the orange luminescence of the complex increased progressively. After 6.5 h, the mixture was concentrated under reduced pressure to remove most of the THF prior to purification by dialysis, which was performed against water with a 50 kDa cutoff dialysis tube (Spectrapore) for four days at room temperature. Finally, the dialyzed solution was lyophilized, affording a luminescent fluffy yellow solid. UV−vis (H_2O) MLCT absorptions: λ_{abs} 378 nm (ε = 4310 M^{-1} cm^{-1}) and 417 nm (ε = 2300 M^{-1} cm^{-1}). ^{1}H NMR (D_2O, 300 K, 9.4 T), majority part signals: δ 8.85 (1H, NHCO(4)), 8.75 (1H, NHCO(7)), 5.49 (1H, CH(5)), 3.49 (1H, CH$_2$(1)), 3.46 (1H, CH$_2$(12)), 3.40−3.20 (accidentally overlapped signals: 1H, CH$_2$(13); 1H, CH(15); 1H, CH(16)), 3.19−3.04 (accidentally overlapped signals: 1H, CH$_2$(1); 1H, CH(10)), 3.03 (1H, CH$_2$(12)), 2.87 (1H, CH$_2$(13)), 2.71 (1H, CH$_2$(16)), 2.66 (2H, CH$_2$(2)), 2.60 (2H, CH$_2$(9)). ^{13}C NMR (D_2O, 300 K, 9.4 T): δ 58.2 (CH(5)), 56.4 (CH(15)), 55.5 (CH$_2$(16)), 52.1 (CH$_2$(10)), 49.3 (CH$_2$(13)), 48.9 (CH$_2$(12)), 48.1 (CH$_2$(1)), 30.6 (CH$_2$(9)), 30.0 (CH$_2$(2)), 13.9 (CH$_3$(17)). Elemental analysis: Anal. Calcd for $(C_{13}H_{22}N_4O_4)_{0.94}$ $(C_{24}H_{27}N_5O_4)_{0.06}$ $(C_{22}H_{16}ClN_2Ir)_{0.053}$ $(H_2O)_2$ $(CF_3SO_3H)_{0.3}$: C, 43.58; H, 6.64; N, 14.00; Ir, 2.44. Found: C, 43.83; H, 6.77; N, 14.18; Ir, 2.45. The Ir content was measured by ICP-AES spectroscopy after a known amount of lyophilized polymer was digested in a mixture of concentrated HCl and HNO_3 in a 1:1 ratio for 24 h at room temperature.

4.5. Photochemical Stability of $\mathbf{1_M}$ and $\mathbf{1_P}$. A sample of $\mathbf{1_P}$ (0.8 mg) was dissolved in 2.5 mL of an H_2O/MeOH (85:15) mixture, corresponding to [Ir] = 4.1 × 10^{-5} M. After saturation by O_2 (bubbled directly into the cuvette for 10−15 min), the solution was irradiated through a cutoff optical filter (>390 nm) for 240 min overall, and UV−vis absorption spectra were collected after 30, 60, 90, 180, and 240 min of irradiation. The same procedure was employed for compound $\mathbf{1_M}$ in the solution obtained by dissolving 2.6 mg of **1** in 10 mL of an H_2O/MeOH (85:15) mixture, and then diluting the solution 1:10 (final [$\mathbf{1_M}$] = 3.3 × 10^{-5} M).

4.6. Photoreaction of $\mathbf{1_M}$ and $\mathbf{1_P}$ with DHN. In a volumetric flask (10 mL), 3.2 mg of $\mathbf{1_M}$ (4.1 × 10^{-3} mmol) was dissolved in an H_2O/MeOH (85:15) mixture containing 6.0 mg of DHN (3.7 × 10^{-3} mmol). This solution was diluted 1:10 to obtain a final [$\mathbf{1_M}$] = 4.1 × 10^{-5} M and [DHN] = 3.7 × 10^{-4} M. Before irradiation, the solution was saturated with O_2 by bubbling directly in the cuvette for 10 min. The solution was then irradiated through a cutoff optical filter (>390 nm) for a total of 150 min, while spectra were recorded every 5 min for the first hour, then at 90, 120, and 150 min. The same procedure was followed for the photoreaction involving $\mathbf{1_P}$ using 0.7 mg of $\mathbf{1_P}$ (8.9 × 10^{-5} mmol of Ir) in 2.5 mL of the H_2O/MeOH mixture containing DHN ([Ir] bound to PhenISA = 3.6 × 10^{-5} M).

The ratio between the quantum yields for $^1O_2$ generation by $\mathbf{1_M}$ and $\mathbf{1_P}$ was evaluated on the basis of the following considerations. The rate of the photochemical reaction (r) is expressed by eq 3, where ϕ is the quantum yield of the reaction and I indicates the photons absorbed by the reactant.[48]

$$r = \phi I \tag{3}$$

The ratio between the quantum yields for $^1O_2$ generation is therefore given by eq 4.

$$\frac{\phi_{\mathbf{1_M}}}{\phi_{\mathbf{1_P}}} = \frac{r_{\mathbf{1_M}}}{r_{\mathbf{1_P}}} \times \frac{I_{\mathbf{1_P}}}{I_{\mathbf{1_M}}} \tag{4}$$

For monochromatic excitation, the ratio I_{1_P}/I_{1_M} can be computed by eq 5, where $I°$ indicates the incident photon flux and $A(\mathbf{1_P})$ and $A(\mathbf{1_M})$ indicate the absorbance of the two complexes at the excitation wavelength.

$$\frac{I_{\mathbf{1_P}}}{I_{\mathbf{1_M}}} = \frac{I°_{\mathbf{1_P}}(1 - 10^{-A(\mathbf{1_P})})}{I°_{\mathbf{1_M}}(1 - 10^{-A(\mathbf{1_M})})} \tag{5}$$

In our case, multichromatic excitation by a filtered lamp was employed, and then integration over the entire spectral range (λ = 390−600 nm) was performed on the reduced fraction obtained by considering that the incident photon fluxes ($I°$) were identical in the two experiments. Thus, the ratio I_{1_P}/I_{1_M} was calculated to be 0.89.

As to the r_{1_M}/r_{1_P} term, the starting concentration of DHN was the same in the two experiments (Figure 3), and therefore the ratio between the initial reaction rates is given simply by the ratio of k_{obs} for $\mathbf{1_M}$ and $\mathbf{1_P}$ (i.e., 2.4). This ratio should hardly be affected by the fact that absorbance outside the linear range of the Lambert−Beer relationship was used in the first-order plots affording k_{obs} (Figures 2 and 3). In fact, the inaccuracy is expected to be the same for both $\mathbf{1_M}$ and $\mathbf{1_P}$ because the reactant was the same (DHN), and the range of the spanned absorbances was very similar in the two cases.

Therefore, ϕ_{1_M}/ϕ_{1_P} = 2.4 × 0.89 = 2.1.

4.7. Cell Culture and Treatment. The HeLa cell line[49] was cultured at 37 °C with 5% CO_2 in complete DMEM (10% FBS, 2 mM L-glutamine, 10 mM HEPES, 100 μM nonessential amino acids, and penicillin plus streptomycin). Cultures at ∼80% confluence were routinely split 1:10 in 10 cm culture dishes. Cell cultures that were 70−80% confluent were incubated with either $\mathbf{1_M}$ or $\mathbf{1_P}$ in DMEM plus 1% FBS. After incubation, the cells were washed three times in PBS, and then complete DMEM was added.

4.8. TPE Measurements and Cellular Uptake. The laser source was a mode-locked Ti:sapphire laser (Mai Tai HP, Spectra Physics) with pulses of 120 fs full width at half-maximum and 80 MHz repetition frequency. The optical setup was built around a confocal scanning head (FV-300, Olympus) mounted on an upright optical microscope (BX51, Olympus) equipped with a high working distance

DOI: 10.1021/ic502378z
Inorg. Chem. XXXX, XXX, XXX−XXX

objective (NA = 1.1, wd = 2 mm, 60×, water immersion, Olympus). Nonconfocal TPE imaging was performed using the FV-300 scanning unit after removing the largest pinhole from the pinhole wheel. The objective simultaneously focused the laser beam on the sample and collected the signal in epifluorescence geometry through the non-descanned collection channels described hereafter. The non-descanned detection system (ND unit) collected the emitted light right above the microscope objective lens, thereby avoiding the complex optical path back to the photomultipliers in the FV-300 scanning head. The signal reaching the ND unit is fed to three Hamamatsu analog output photomultipliers (HC125-02, Hamamatsu) whose 21 mm diameter photocathode ensured the collection of most of the light during scanning. The ND unit has been designed to minimize the distance between the entrance pupil of the objective and the active area of the detector. The fluorescence signal was filtered by 485/50, 535/50, and 600/40 band-pass filters to select the fluorescence light and remove scattering and undesired autofluorescence from the sample, and it was processed by means of Fluoview 5.0 software (Olympus).

Images were recorded at different times after the addition of the Ir complexes (~2 h for $\mathbf{1}_M$, 100 μL of a 5.5×10^{-4} M solution affording a 26 μM concentration in the well; ~12 h for $\mathbf{1}_P$, 100 μL of a 4.7×10^{-4} M solution affording a 22 μM concentration in the well). Two-photon excitation at 840 nm was exploited (with an excitation power of 15 mW). Autofluorescent bleed through was verified on nonstained samples by measuring fluorescence emission in the presence and absence of the band-pass filter selecting the emission of the samples. Images shown in this Article are the result of 2 kalman average scans with 10 or 6 μs of residence time per pixel, depending on the zoom factor. The field of view of the 512 × 512 pixel images was 157 × 157 μm^2 or 79 × 79 μm^2, as indicated in the caption of Figure 4.

4.9. Flow Cytometry. After treatment for 4 and 6 h, the adherent cells were harvested from the culture dishes with trypsin-EDTA (Euroclone) and collected in complete DMEM, washed 3 times in fluorescence-activated cell-sorting (FACS) buffer containing phosphate buffered solution (PBS) with 2 mM EDTA and 2% fetal bovine serum (FBS), and then processed for the annexin V/7ADD assay (Biolegend) following the manufacturer's instructions. Stained cells (~5×10^4) were acquired with a CANTO II flow cytometer (BD Pharmingen) and analyzed with FlowJo software (Treestar).

4.10. Viability Test in the Dark. HeLa cells at 80% confluency were cultured and treated with $\mathbf{1}_M$ or $\mathbf{1}_P$ as described in section 4.7, and then a trypan blue exclusion test (that selectively stains dead cells) and a Neubauer cell counting chamber were used to count the total cell number and the percentage of dead cells. All conditions were tested in triplicate.

■ ASSOCIATED CONTENT

Supporting Information

The NMR spectra, the absorption and emission data in different solvents, the DLS size distribution profile, the stability test, the microscopy image of the control untreated HeLa cells, the flow-cytometry analysis, the dark toxicity data, and the emission profile of the Xe lamp. This material is available free of charge via the Internet at http://pubs.acs.org.

■ AUTHOR INFORMATION

Corresponding Author

*E-mail: daniela.maggioni@unimi.it. Fax: +390250314405. Phone: +390250314352.

Notes

The authors declare no competing financial interest.

■ ACKNOWLEDGMENTS

The authors warmly thank Dr. Vladimiro Dal Santo for the ICP-AES measurements.

■ REFERENCES

(1) (a) DeRosa, M. C.; Crutchley, R. J. *Coord. Chem. Rev.* **2002**, *233−234*, 351−371. (b) Wang, S.; Gao, R.; Zhou, F.; Selke, M. *J. Mater. Chem.* **2004**, *14*, 487−493. (c) Allison, R. R.; Mota, H. C.; Shibata, C. H. *Photodiagn. Photodyn. Ther.* **2004**, *1*, 263−277. (d) Chatterjee, D. K.; Fong, L. S.; Zhang, Y. *Adv. Drug Delivery Rev.* **2008**, *60*, 1627−1637.

(2) Triesscheijn, M.; Baas, P.; Schellens, J. H.; Stewart, F. A. *Oncologist* **2006**, *11*, 1034−1044.

(3) Rhodes, L. E.; de Rie, M.; Enstrom, Y.; Groves, R.; Morken, T.; Goulden, V.; Wong, G. A.; Grob, J. J.; Varma, S.; Wolf, P. *Arch. Dermatol.* **2004**, *140*, 17−23.

(4) Hur, C.; Nishioka, N. S.; Gazelle, G. S. *Dig. Dis. Sci.* **2003**, *48*, 1273−1283.

(5) Kato, H. *J. Photochem. Photobiol.* **1998**, *B42*, 96−99.

(6) Schuller, D. E.; McCaughan, J. S., Jr.; Rock, R. P. *Arch. Otolaryngol.* **1985**, *111*, 351−355.

(7) Kharkwal, G. B.; Sharma, S. K.; Huang, Y. Y.; Dai, T.; Hamblin, M. R. *Lasers Surg. Med.* **2011**, *43*, 755−767.

(8) Agostinis, P.; Berg, K.; Cengel, K. A.; Foster, T. H.; Girotti, A. W.; Gollnick, S. O.; Hahn, S. M.; Hamblin, M. R.; Juzeniene, A.; Kessel, D.; Korbelik, M.; Moan, J.; Mroz, P.; Nowis, D.; Piette, J.; Wilson, B. C.; Golab, J. *CA−Cancer J. Clin.* **2011**, *61*, 250−281.

(9) For example: (a) Mroz, P.; Yaroslavsky, A.; Kharkwal, G. B.; Hamblin, M. R. *Cancers* **2011**, *3*, 2516−2539. (b) Allison, R. R.; Moghissi, K. *Clinical Endoscopy* **2013**, *46*, 24−29.

(10) Oleinick, N. L.; Morris, R. L.; Belichenko, I. *Photochem. Photobiol. Sci.* **2002**, *1*, 1−21 , and references therein.

(11) (a) Murtinho, D.; Pineiro, M.; Pereira, M. M.; Gonsalves, A. M.; Arnaut, L. G.; Miguel, M. G.; Burrows, H. D. *J. Chem. Soc., Perkin Trans. 2* **2000**, 2441−2447. (b) Horiuchi, H.; Tanaka, T.; Yoshimura, K.; Sato, K.; Kyushin, S.; Matsumoto, H.; Hiratsuka, H. *Chem. Lett.* **2006**, *35*, 662−663. (c) Maeda, D.; Shimakoshi, H.; Abe, M.; Hisaeda, Y. *Inorg. Chem.* **2009**, *48*, 9853−9860.

(12) (a) Ikeda, A.; Sato, T.; Kitamura, K.; Nishiguchi, K.; Sasaki, Y.; Kikuchi, J.; Ogawa, T.; Yogo, K.; Takeya, T. *Org. Biomol. Chem.* **2005**, *3*, 2907−2909. (b) Mroz, P.; Tegos, G. P.; Gali, H.; Wharton, T.; Sarna, T.; Hamblin, M. R. *Photochem. Photobiol. Sci.* **2007**, *6*, 1139−1149.

(13) Tardivo, J. P.; Giglio, A. D.; Oliveira, C. S.; Gabrielli, D. S.; Junqueira, H. C.; Tada, D. B.; Severino, D.; Turchiello, R. F.; Baptista, M. S. *Photodiag. Photodyn. Ther.* **2005**, *2*, 175−191.

(14) Ishiyama, K.; Nakamura, K.; Ikai, H.; Kanno, T.; Kohno, M.; Sasaki, K.; Niwano, Y. *PLoS One* **2012**, *7*, e37871.

(15) Takizawa, S.; Aboshi, R.; Murata, S. *Photochem. Photobiol. Sci.* **2011**, *10*, 895−903.

(16) (a) Djurovich, P. I.; Murphy, D.; Thompson, M. E.; Hernandez, B.; Gao, R.; Hunt, P. L.; Selke, M. *Dalton Trans.* **2007**, 3763−3770. (b) Gao, R.; Ho, D. G.; Hernandez, B.; Selke, M.; Murphy, D.; Djurovich, P. I.; Thompson, M. E. *J. Am. Chem. Soc.* **2002**, *124*, 14828−14829.

(17) (a) Majumdar, P.; Yuan, X.; Li, S.; Le Guennic, B.; Jie Ma, J.; Zhang, C.; Jacqueminde, D.; Zhao, J. *J. Mater. Chem. B* **2014**, *2*, 2838−2854. (b) Nakagawa, A.; Hisamatsu, Y.; Moromizato, S.; Kohno, M.; Aoki, S. *Inorg. Chem.* **2014**, *53*, 409−422. (c) Ye, R.-R.; Tan, C.-P.; He, L.; Chen, M.-H.; Ji, L.-N.; Mao, Z.-W. *Chem. Commun. (Cambridge, U.K.)* **2014**, *50*, 10945−10948. (d) Li, S. P.-Y.; Lau, C. T.-S.; Louie, M.-W.; Lam, Y.-W.; Cheng, S. H.; Lo, K. K.-W. *Biomaterials* **2013**, *34*, 7519−7532. (e) Moromizato, S.; Hisamatsu, Y.; Suzuki, T.; Matsuo, Y.; Abe, R.; Aoki, S. *Inorg. Chem.* **2012**, *51*, 12697−12706.

(18) Sajoto, T.; Djurovich, P. I.; Tamayo, A. B.; Oxgaard, J.; Goddard, W. A.; Thompson, M. E. *J. Am. Chem. Soc.* **2009**, *131*, 9813−9822.

(19) (a) Larson, N.; Ghandehari, H. *Chem. Mater.* **2012**, *24*, 840−853. (b) Soesbe, T. S.; Kiefer, G. E.; Sherry, A. D. *J. Am. Chem. Soc.* **2008**, *130*, 13854−13855. (c) Liu, L.; Li, X.; Hou, S.; Xue, Y.; Yao, Y.; Ma, Y.; Feng, X.; He, S.; Lu, Y.; Wang, Y.; Zeng, X. *Chem. Commun. (Cambridge, U.K.)* **2009**, *44*, 6759−6761. (d) Kim, J. H.; Park, K.;

DOI: 10.1021/ic502378z
Inorg. Chem. XXXX, XXX, XXX−XXX

Nam, H. Y.; Lee, S.; Kim, K.; Kwon, I. C. *Prog. Polym. Sci.* **2007**, *32*, 1031−1053.
(20) (a) Matzumura, Y.; Maeda, H. *Cancer Res.* **1986**, *46*, 6387−6392. (b) Fox, M. E.; Szoka, F. C.; Fréchet, J. M. *Acc. Chem. Res.* **2009**, *42*, 1141−1151. (c) Peer, D.; Karp, J. M.; Hong, S.; Farokhzad, O. C.; Margalit, R.; Langer, R. *Nat. Nanotechnol.* **2007**, *2*, 751−760.
(21) (a) Ferruti, P.; Marchisio, M. A.; Duncan, R. *Macromol. Rapid Commun.* **2002**, *23*, 332−355. (b) Ranucci, E.; Ferruti, P.; Lattanzio, E.; Manfredi, A.; Rossi, M.; Mussini, P. R.; Chiellini, F.; Bartoli, C. *J. Polym. Sci., Part A: Polym. Chem.* **2009**, *47*, 6977−6991.
(22) (a) Cavalli, R.; Bisazza, A.; Sessa, R.; Primo, L.; Fenili, F.; Manfredi, A.; Ranucci, E.; Ferruti, P. *Biomacromolecules* **2010**, *11*, 2667−2674. (b) Ferruti, P.; Franchini, J.; Bencini, M.; Ranucci, E.; Zara, G. P.; Serpe, L.; Primo, L.; Cavalli, R. *Biomacromolecules* **2007**, *8*, 1498−1504.
(23) Donghi, D.; Maggioni, D.; D'Alfonso, G.; Amigoni, F.; Ranucci, E.; Ferruti, P.; Manfredi, A.; Fenili, F.; Bisazza, A.; Cavalli, R. *Biomacromolecules* **2009**, *10*, 3273−3282.
(24) Maggioni, D.; Fenili, F.; D'Alfonso, L.; Donghi, D.; Panigati, M.; Zanoni, I.; Marzi, R.; Manfredi, A.; Ferruti, P.; D'Alfonso, G.; Ranucci, E. *Inorg. Chem.* **2012**, *51*, 12776−12788.
(25) Richardson, S.; Ferruti, P.; Duncan, R. *J. Drug Targeting* **1999**, *6*, 391−404.
(26) Lowry, M. S.; Hudson, W. R.; Pascal, R. A., Jr.; Bernhard, S. *J. Am. Chem. Soc.* **2004**, *126*, 14129−14135.
(27) Wang, Z.; McWilliams, A. R.; Evans, C. E. B.; Lu, X.; Chung, S.; Winnik, M. A.; Manners, I. *Adv. Funct. Mater.* **2002**, *12*, 415−419.
(28) Zhao, Q.; Liu, S.; Shi, M.; Li, F.; Jing, H.; Yi, T.; Huang, C. *Organometallics* **2007**, *26*, 5922−5930.
(29) The term "solvent's polarity" is usually employed for describing the capacity of a solvent for solvating dissolved charged or dipolar species.[30] Although this is easy to understand qualitatively, substantial difficulties are encountered on attempting a more precise/comprehensive definition of "polarity" or its quantitative measures. Many semiempirical solvent polarity scales have been developed,[30] and some of them are derived from spectroscopic measurements, such as the well-known $E_T(30)$ scale.[31]
(30) Katritzky, A. R.; Fara, D. C.; Yang, H.; Tämm, K.; Tamm, T.; Karelson, M. *Chem. Rev.* **2004**, *104*, 175−198.
(31) Reichardt, C. *Solvents and Solvent Effects in Organic Chemistry*, 3rd ed.; Wiley-VCH Publishers: Weinheim, Germany, 2003.
(32) Giordano, P. J.; Wrighton, M. *J. Am. Chem. Soc.* **1979**, *101*, 2888−2897.
(33) Lakowicz, J. R. *Principles of Fluorescence Spectroscopy*, 2nd ed.; Kluwer Academic/Plenum Publishers: New York, 1999; Chapter 6, p 185.
(34) Lo, K. K.-W.; Ng, D. C.-M.; Chung, C.-K. *Organometallics* **2001**, *20*, 4999−5001, and references therein.
(35) For example: Mauro, M.; De Paoli, G.; Otter, M.; Donghi, D.; D'Alfonso, G.; De Cola, L. *Dalton Trans.* **2011**, *40*, 12106−12116.
(36) For example: Rampazzo, E.; Bonacchi, S.; Montalti, M.; Prodi, L.; Zaccheroni, N. *J. Am. Chem. Soc.* **2007**, *129*, 14251−14256.
(37) Yersin, H.; Rausch, A. F.; Czerwieniec, R.; Hofbeck, T.; Fischer, T. *Coord. Chem. Rev.* **2011**, *255*, 2622−2652.
(38) Wrighton, M.; Morse, D. L. *J. Am. Chem. Soc.* **1974**, *96*, 998−1003.
(39) For example: (a) Lees, A. J. *Coord. Chem. Rev.* **1998**, *177*, 3−35. (b) Li, M.-J.; Chen, Z.; Yam, V. W.-W.; Zu, Y. *ACS Nano* **2008**, *2*, 905−912.
(40) Wu, W.; Yang, P.; Ma, L.; Lalevée, J.; Zhao, J. *Eur. J. Inorg. Chem.* **2013**, 228−231.
(41) Stratakis, M.; Orfanopoulos, M. *Tetrahedron* **2000**, *56*, 1595−1615.
(42) (a) Fernandez-Moreira, V.; Thorp-Greenwood, F. L.; Coogan, M. P. *Chem. Commun. (Cambridge, U.K.)* **2010**, *46*, 186−202. (b) Mari, C.; Panigati, M.; D'Alfonso, L.; Zanoni, I.; Donghi, D.; Sironi, L.; Collini, M.; Maiorana, S.; Baldoli, C.; D'Alfonso, G.; Licandro, E. *Organometallics* **2012**, *31*, 5918−5928.
(43) Lo, K. K.-W.; Lee, P.-K.; Lau, J. S.-Y. *Organometallics* **2008**, *27*, 2998−3006.
(44) Strassert, C. A.; Mauro, M.; De Cola, L. *Adv. Inorg. Chem.* **2011**, *63*, 47−103.
(45) Ferruti, P.; Ranucci, E.; Trotta, F.; Gianasi, E.; Evagorou, G. E.; Wasil, M.; Wilson, G.; Duncan, R. *Macromol. Chem. Phys.* **1999**, *200*, 1644−1654.
(46) Sprouse, S.; King, K. A.; Spellane, P. J.; Watts, R. J. *J. Am. Chem. Soc.* **1984**, *106*, 6647−6653.
(47) Ishida, A.; Tobita, S.; Hasegawa, Y.; Katoh, R.; Nozaki, K. *Coord. Chem. Rev.* **2010**, *254*, 2449−2458.
(48) Balzani, V.; Carassiti, V. *Photochemistry of Coordination Compounds*; Academic Press: London and New York, 1970.
(49) Scherer, W. F.; Syverton, J. T.; Jey, G. O. *J. Exp. Med.* **1953**, *97*, 695−710.

DOI: 10.1021/ic502378z
Inorg. Chem. XXXX, XXX, XXX−XXX